DOI: 10.1002/ejoc.200501012

Synthesis and Conformational Analysis of Galactose-Derived Bicyclic Scaffolds

Silvia Mari,[a] F. Javier Cañada,[a] Jesús Jiménez-Barbero,*[a] Anna Bernardi,*[b] Gilles Marcou,[b] Ilaria Motto,[b] Ingrid Velter,[c] Francesco Nicotra,*[c] and Barbara La Ferla[c]

Keywords: NMR spectroscopy / Molecular modelling / Carbohydrates / Carbohydrate mimics

Two novel galactose-derived bicyclic acetamides were synthesized. The conformational behavior of these cyclic acetamides in aqueous solution was fully investigated. The NMR spectroscopic data suggests that the pyran ring interconverts between two ($^4C_1$, $^1S_3$) or three ($^4C_1$, $^1S_3$ and $^1C_4$) conformations and molecular modelling studies allowed the structures' geometries to be defined. Three different force fields were used (Amber*, MM3* and OPLSAA) and fitting procedures were employed to reproduce the experimental $^3J_{H-H}$ coupling constants and NOE contacts. Evaluation of the results established which of these three well-known force fields were the most reliable in reproducing the experimental observations and should therefore be used for analogous design studies.

Introduction

Carbohydrates can be regarded as ideal scaffolds for library generation:[1–4] they are mainly polyhydroxylated (but they also bear amino and carboxy functionalities) and each group has a well defined orientation enforced by the conformational constraints of the cyclic structure. However, natural carbohydrates are non-original scaffolds and their chemical and metabolic stability is not very high. The chemical modification of carbohydrates can afford original, stable and possibly more rigid compounds. Such structures can be decorated by appending diverse pharmacophores to their functional groups. For practical purposes it is important that the new scaffolds be readily accessible on a large scale at a limited cost. Information about their structure and dynamics in aqueous solution is also very valuable for structure-based (drug) design projects and for the rational design of individual ligands and libraries thereof. In this context, where computational tools are required, their ability to render the three-dimensional structure of the scaffolds should be validated against available experimental data, before embarking on subsequent molecular design projects.

In the course of collaboration within an European Research Network we have developed a short synthesis of the functionally rich bicyclic structures **1** and **2** (Scheme 1). These molecules are easily obtained from galactose in four steps, without the need of protecting group chemistry (see below) and can be variously functionalized at the appended side-chain. Both characteristics make them particularly attractive for further (combinatorial) development. To fully exploit their potential, the conformational analysis of these

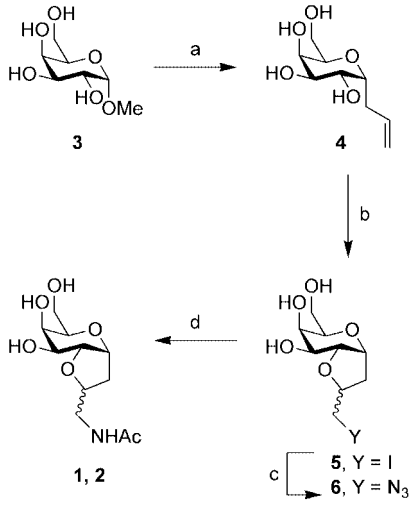

Scheme 1. a) i. BTSFA, CH_3CN, reflux, 1 h; ii. allyltrimethylsilane, TMSOTf (0.5 equiv.), 0 °C–room temp., 18 h, 85%; b) I_2, $NaHCO_3$, DMF, room temp., 12 h, 84%; c) nBu_4NN_3, DMF, room temp., 14 h, 75%; d) H_2, $Pd(OH)_2$/C, Ac_2O, MeOH, room temp., 24 h 70%.

[a] Departamento de Estructura y Funcion de Proteinas, Centro de Investigaciones Biologicas CSIC,
c/Ramiro de Maeztu 9, 28040 Madrid, Spain
Fax: +34-91-536-0432
E-mail: jjbarbero@cib.csic.es
[b] Dipartimento di Chimica Organica e Industriale e Centro di Eccelenza CISI, Università degli Studi di Milano,
Via Venezian 21, 20133 Milano, Italy
Fax: +39-02-503-14092
E-mail: anna.bernardi@unimi.it
[c] Dipartimento di Biotecnologie e Bioscienze, Università degli Studi di Milano Bicocca,
Piazza della Scienza 2, 20126 Milano, Italy
Fax: +39-02-6448-3519
E-mail: francesco.nicotra@unimib.it
Supporting information for this article is available on the WWW under http://www.eurjoc.org or from the author.

molecules in the free state was performed by combining NMR and modelling data. The results are reported in this paper.

Results

Synthesis

The preparation of the bicyclic acetamides **1** and **2** was started from the commercially available methyl α-D-galactopyranoside **3** (Scheme 1), according to a procedure described by Gray and co-workers.[5,6] Silylation of **3** using bis(trimethylsilyl)trifluoroacetamide (BTSFA) was followed by in situ treatment with allyltrimethylsilane and catalytic trimethylsilyl trifluoromethanesulfonate[7] to afford the α-*C*-allyl galactosyl **4** as a single diastereomer. The stereochemistry of **4** was assigned after acetylation on the basis of the $J_{H1–H2}$ coupling constant (4.8 Hz).

Iodocyclization of compound **4** provided a 2.6:1 inseparable mixture of diastereomeric iodides **5**,[8,9] which was then submitted for azide displacement to afford the bicyclic azides **6**. Hydrogenation of this mixture, over 20% $Pd(OH)_2$/C in methanol and in the presence of acetic anhydride at atmospheric pressure, afforded a mixture of the bicyclic acetamides **1** and **2**, which were separated by HPLC using a Waters high performance carbohydrate 60 Å column. The synthesis of compounds **1** and **2** was thus performed without the use of protection/deprotection chemistry, in four steps and 25% and 12% overall yield, respectively.

Conformational Studies

NMR Data

In order to define their three-dimensional structure and dynamics, **1** and **2** were subjected to NMR studies in D_2O solutions at 400 MHz and 500 MHz. Both coupling constant analysis (Table 1) and NOE data (Table 2) suggested that the bicyclic cores of both compounds exist in multiple conformations. In particular, the data obtained for the six-membered ring protons are clearly not consistent with the single $^4C_1$ chair that is usually adopted by *galacto*-pyran: the observed $J_{2,3}$ values are too small and the $J_{4,5}$ values are too large (Table 1). Consistently, the H3–H5 NOE cross peaks are weaker than expected for a typical $^4C_1$ pyran ring and the H1–H6*proR* proton pair gives rise to medium intensity NOE contacts which are not compatible with a $^4C_1$ ring conformation (Table 2). Hence, the 1,2-*cis*-fused furan ring appears to distort the six-membered ring of both **1** and **2** out of the usual *galacto*-pyran conformation by a measurable extent.

The orientation of the hydroxy methyl group tethered to the pyran ring was also investigated. As expected for galactose, the measured coupling constants were consistent with a preferred *gt* rotamer (ω = +60°, see Supporting Information, SI-2 and SI-Table 6).[10]

Table 1. Experimental $^3J_{HH}$ values for compounds **1** and **2**.

Protons pairs	Exp. $^3J_{H–H}$ (Hz) for **1**	Exp. $^3J_{H–H}$ (Hz) for **2**
H1–H2	6.6	5.9
H2–H3	6.4	6.7
H3–H4	2.8	3.0
H4–H5	2.8	3.2
H1–H3′*proS*	6.6	6.9; 5.3[a]
H1–H3′*proR*	6.6	6.9; 5.3[a]
H4′–H3′*proS*	6.8; 7.8[a]	7,4; ?[a]
H4′–H3′*proR*	6.8; 7.8[a]	7,4; ?[a]
H5–H6*proS*	8.9	8.5
H5–H6*proR*	3.7	3.5

[a] The scalar coupling between these proton pairs could not be assigned: the corresponding values were not used in the following fitting procedure.

Table 2. Experimentally observed NOE contacts.

Compound	Proton pair	Exp. NOE (%)[a]
1	H1–H4′	2.30
	H3′*proS*–H3	3.70
	H3′*proS*–H5	7.09
	H3–H5	3.24
	H1–H6*proR*	3.01
	H4′–H2	2.72
2	H1–H3′*proR*	3.94
	H1–H3′*proS*	0.43
	H1–H6*proR*	2.89
	H5–H3	3.43
	H4′–H3	2.14
	H6*proS*–H4	2.61
	H3′*proS*–H3	1.93
	H3′*proS*–H5	5.10
	H3′*proR*–H2	1.28

[a] Exp. NOE (%) was calculated as percentage of the cross-peak relative to its corresponding diagonal peak.

Modelling Results

In order to identify the other accessible conformations, conformational analyses of **1** and **2** were performed by molecular mechanics (MM), using three different force fields (AMBER*, MM3* and OPLSAA)[11] and the implicit water salvation model GB/SA[12] of Macromodel.[13] MM3 is a general purpose force field (FF), which is well parameterized for many classes of compounds including sugars.[14] AMBER* has a very good set of parameters for carbohydrates and is our FF of choice for MM calculations on sugars.[15] OPLSAA, a very popular high-quality force field, was chosen as an alternative.

A conformational search was performed using the MC/EM protocol[16] and the resulting conformations, within 12.6 kJ/mol from the global minimum, were clustered for each molecule based on the values of two dihedral angles of the ring τ_1 and τ_4 (C1–C2–C3–C4 and C1–O–C5–C4), respectively (see Figure 1). Structures were classified as skew-boat (S), chair ($^4C_1$), or inverted chair ($^1C_4$) conformations of the pyran moiety.[17] The bicycle conformations of the cluster leaders were found to be independent of the configuration of the stereocenter at C4′ and hence basically identical for both **1** and **2**. The results turned out to be highly force field dependent (for details, see the Conforma-

tional Analysis section in the Supporting Information) and are illustrated in Figure 2, which shows the leading members of the clusters found by the three different force fields, their relative energy and their Boltzmann distribution at room temperature.

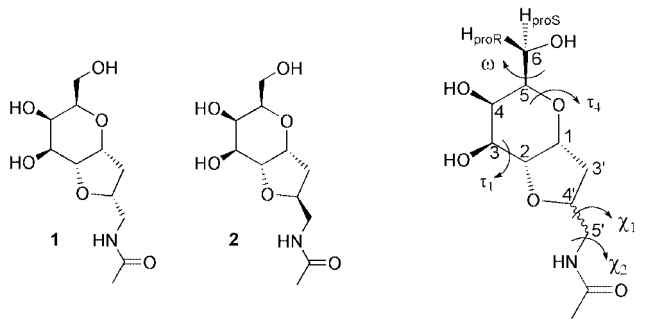

Figure 1. Structures of compounds **1** and **2**, atom numbering and definitions of dihedral angles ω, τ_4, τ_1, χ_1 and χ_2 as $OC_5C_6O_6$, $C_1OC_5C_4$, $C_1C_2C_3C_4$ and $O'C_{4'}C_{5'}N$, $C_{4'}C_{5'}NC(O)$, respectively.

For each force field a different conformation is calculated to represent at least 92% of the global population, as based on the Boltzmann distribution at room temperature (Figure 2, last column). AMBER* favors a $^4C_1$ chair, MM3* the $^1S_3$ skew-boat and OPLSAA a $^1C_4$ chair. Each conformation of the pyran ring is associated with multiple folds of the five-membered ring and multiple conformations of the pending side chain, which are described in detail in the Supporting Information section. Here we will only note that for **1** the $^1S_3$ cluster structures calculated by AMBER* and those calculated by MM3* are associated with different folds of the five-membered ring. From Figure 2 it can also be noted that the *gt* orientation of the hydroxy methyl group is correctly reproduced by AMBER* and OPLSAA, but conspicuously not by MM3* (see the cluster leaders in Figure 2).

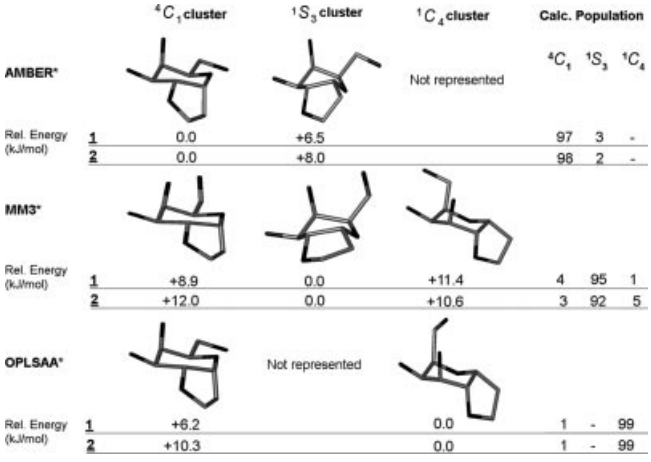

Figure 2. MC/EM search of **1** and **2**: clustering of the pyran ring. Leading members of the clusters found by the three different force fields are shown, together with their relative energies (kJ/mol).

None of the force field representations can reproduce the experimental observations. For instance, based on the population distributions of Figure 2 the diagnostic $J_{4,5}$ coupling constants for **1** would be 0.9 Hz (AMBER*), 4.2 Hz (MM3*) and 5.9 Hz (OPLSAA), respectively for the three force fields, none of which agrees with the measured value of 2.8 Hz (see Table 1). Analogous considerations can be extended to **2**. Similarly, the NOE data estimated by a full-matrix relaxation approach,[18] (using the Noeprom software[19]) from the calculated structures and relative energies, did not reproduce the experimentally observed cross peak intensities (full details are collected in Tables SI-3 and SI-4 in the Supporting Information) The use of dynamics simulations did not improve the fitting, suggesting that the problem is not caused by improper simulation of the dynamic behavior of the bicycles, but rather by a poor representation of the actual potential energy surface by all of the force fields examined. We therefore decided to use the calculated geometries as templates and to extract their relative populations from the experimental data by a fitting procedure based upon both the coupling constant values and the intensity of the NOE cross peaks.

Coupling Constant Fitting

As discussed above, depending on the force field (AMBER*, MM3*, or OPLSAA) different conformations of the six- and five-membered rings were predicted. Furthermore, the fold of the fused five-membered ring appears to depend upon the conformation of the pyran moiety. With AMBER*, MM3* and OPLSAA geometries at hand, average $^3J_{H-H}$ values were calculated for each cluster of conformers by applying the empirical generalization of the Karplus equation, proposed by Haasnoot et al.,[20] to the corresponding proton–proton torsion angles. The cluster-averaged *J* values (see Table SI-5 in the Supporting Information) were found to be somewhat force field dependent, particularly for the five-membered ring protons, thus reflecting the different five-membered ring folds located by each force field. These values were used to obtain the relative population of each cluster by fitting to the experimental $^3J_{HH}$ values. This procedure accounted for the different five-membered ring puckerings represented in each cluster. We felt that this procedure was more robust than the alternative possibility of using only the cluster leader geometry as representative of each cluster in the fitting process. An initial value was assigned to the weight of each cluster and an estimation of the scalar couplings calculated. Subsequently, the deviation between the calculated and experimental scalar couplings was iteratively minimized (up to 10.000 steps), thus obtaining the best-fitting population weights. The relative populations of the clusters obtained by this fitting procedure (*J*-fitted populations) are reported in Table 3 (cluster *J*-fitted ratio row) together with their associated scalar coupling constant values ($^3J_{H-H}$) for each proton pair compared to the experimental values. According to AMBER*, the experimental coupling constant values measured for **1** were best fitted by a 60:40 ratio of $^4C_1$:$^1S_3$ conformations. The associated $^3J_{H-H}$ ($^3J_{H-H}$ Amber* fitting column) values are in good agreement with the measured values and the calculated agreement factor is 0.52 Hz (agreement factor is calculated as the sum of deviations di-

Table 3. Experimental and estimated $^3J_{HH}$ values for compounds **1** and **2**.

Compound	Protons pairs	Exp. $^3J_{H-H}$ (Hz)	$^3J_{H-H}$ Amber* fitting (Hz)[a]	$^3J_{H-H}$ MM3* fitting (Hz)[a]	$^3J_{H-H}$ OPLSAA fitting (Hz)[a]
Cluster *J*-fitted ratio[b]			$^4C_1$:$^1S_3$, 60:40	$^4C_1$:$^1S_3$:$^1C_4$, 48:25:27	$^4C_1$:$E_{3'}$:$^1C_4$, 60:0:40
1	H1–H2	6.6	5.4	5.3	5.1
	H2–H3	6.4	7.2	6.3	5.2
	H3–H4	2.8	2.6	2.7	3.7
	H4–H5	2.8	2.1	2.9	2.8
	H1–H3′*proS*	6.6	6.3	6.8	6.4
	H1–H3′*proR*	6.6	6.3	6.7	7.0
	H4′–H3′*proS*	6.8; 7.8[c]	7.2	8.8	6.4
	H4′–H3′*proR*	6.8; 7.8[c]	6.9	6.2	8.9
Cluster *J*-fitted ratio[b]			$^4C_1$:$^1S_3$, 45:55	$^4C_1$:$^1S_3$:$^1C_4$, 60:24:16	$^4C_1$:$^1C_4$, 80:20
2	H1–H2	5.9	5.3	5.9	5.9
	H2–H3	6.7	7.0	6.5	6.3
	H3–H4	3.0	2.5	3.0	3.6
	H4–H5	3.2	2.4	1.9	1.8
	H1–H3′*proS*	6.9; 5.3[c]	5.9	6.2	6.9
	H1–H3′*proR*	6.9; 5.3[c]	5.2	5.9	7.3
	H4′–H3′*proS*	7,4; ?[c]	7.4	8.7	7.4
	H4′–H3′*proR*	7,4; ?[c]	6.6	7.2	7.3

[a] Scalar coupling estimated for the *J*-fitted cluster ratio shown below. [b] Conformer distribution obtained by coupling constant fitting using the force field geometry. [c] The scalar coupling between these proton pairs could not be assigned: the corresponding values were not used in the fitting procedure.

vided by the sum of experimental values). In contrast, fitting based on the structures calculated by MM3* led to a relative populations 48:25:27 for the $^4C_1$:$^1S_3$:$^1C_4$ conformers. In this case, the agreement factor is 0.43 Hz. Finally, for the OPLSAA structures the best fit of the experimental values is obtained by 60:40 ratio of the $^4C_1$ and $^1C_4$ clusters. The agreement factor in this case is the worst value and corresponds to 0.71 Hz.

Similar results were obtained for compound **2** (Table 3). With Amber*, the fitted $^4C_1$:$^1S_3$ ratio is 45:55 and the corresponding agreement factor is 0.51 Hz; the MM3* fitted ratio is 60:24:16 for $^4C_1$:$^1S_3$:$^1C_4$ with an agreement factor of 0.38 Hz whilst with OPLSAA the fitting gave 80: 20 for $^4C_1$:$^1C_4$ (agreement factor 0.55 Hz). For comparison, the agreement factors calculated using the populations in Figure 2 are 1.05 Hz (Amber*), 1.53 Hz (MM3*) and 2.21 Hz (OPLSAA) for compound **1** and the corresponding deviations for compound **2** are: 0.84 Hz, 0.90 Hz and 1.98 Hz (for details, see Table SI-3 in the Supporting Information).

Thus, the experimental results can be reproduced with different sets of conformations. In all cases the $^4C_1$ chair is found to be the major isomer and represents 45%–80% of the global conformer population. However, the *J* analysis alone does not allow discrimination amongst force fields.

NOE Contact Analysis

As discussed in the preceding sections, the three force fields have predicted strikingly different mixtures of $^4C_1$, $^1S_3$ and $^1C_4$ conformations. As additional evidence for the presence and characterization of these equilibria, NOE-based analysis was also performed using the set of NOE contacts collected in Table 2. These contacts were selected because they were identified as exclusive for specific clusters, as shown in Tables 4, 5 and 6. The force field-predicted interproton distances and NOE intensities (%) for each cluster were derived using a full-matrix relaxation calculation[15] extended to all the members of each cluster (Tables 4, 5 and 6 Noeprom columns). Again these values are somewhat force field dependent; however some generalizations can be drawn. For the (4′-R) isomer **1** the H1–H4′, H3–H3′*proS* and H5–H3′*proS* NOE contacts are exclusive for the $^4C_1$ cluster, whereas the H1–H6*proR* contact is exclusive for either the skew-boat or the inverted chair families (Figure 3). Contact H2–H4′ is highly enhanced in the $^1S_3$ cluster relative to the $^4C_1$, while the H3–H5 distance is similar in both the chair and skew-boat conformations (around 2.5 and 2.7 Å respectively), but is much longer for the inverted chair $^1C_4$ cluster (> 4.2 Å). In the case of the (4′-S) compound **2** the exclusive NOE contacts for the $^4C_1$ family are H4′–H3, H3–H3′*proS* and H5–H3′*proS*, while for the $^1S_3$ cluster they are H1–H6*proR* and H2–H3′*proR*. Again, the H3–H5 distance is similar in both the chair and skew-boat conformations (around 2.5 and 2.7 Å respectively), but is much longer for the inverted chair $^1C_4$ cluster (> 4.2 Å).

Finally, the conformer distribution was estimated by fitting the Noeprom-based% NOE intensities to the experimental ones. As described for the *J*-fitting procedure, an initial value was assigned to the weight of each cluster and an estimation of the total% NOE intensity was calculated. Subsequently, the deviation between the calculated and experimental values was iteratively minimized (up to 10.000 steps) and thus the best-fitting population weights were obtained. As observed above for the *J*-fitting process, a simpler procedure could have used the leader geometry as representative of each cluster in the fitting process. However, using cluster-averaged NOE intensities as a representation of each cluster accounts for the different five-membered ring puckerings represented in each cluster. The populations

Table 4. Use of the experimental NOE intensities to estimate the relative population of the AMBER* conformations.

Compound	Proton pair	Noeprom Amber*, $^4C_1$, NOE (%)[a] (distance [Å])[b]	Noeprom Amber*, $^1S_3$, NOE (%)[c] (distance [Å])[b]	Exp. NOE (%)	Amber*, fitted NOE (%)[e]
NOE fitted ratio					$^4C_1$:$^1S_3$, 57:43 (*J*-fitted 60:40) [d]
1	H1–H4′	3.48 (2.62)	0.00 (4.01)	2.30	1.97
	H3′*proS*–H3	8.55 (2.42)	0.00 (4.63)	3.70	4.85
	H3′*proS*–H5	12.49 (2.25)	0.00 (4.54)	7.09	7.09
	H3–H5	4.20 (2.50)	2.63 (2.71)	3.24	3.52
	H1–H6*proR*	0.00 (4.69)	3.30 (2.57)	3.01	1.43
	H4′–H2	0.58 (3.51)	0.94 (3.32)	2.72	0.74
NOE fitted ratio					$^4C_1$:$^1S_3$, 40:60 (*J*-fitted 45:55) [d]
2	H1–H3′*proR*	4.31 (2.40)	4.69 (2.38)	3.94	4.54
	H1–H3′*proS*	0.46 (2.95)	1.57 (2.70)	0.43	1.13
	H1–H6*proR*	0.00 (4.69)	3.92 (2.51)	2.89	2.36
	H5–H3	4.88 (2.52)	3.12 (2.71)	3.43	3.82
	H4′–H3	1.90 (2.92)	0.94 (3.34)	2.14	1.32
	H6*proS*–H4	3.44 (2.71)	2.37 (2.88)	2.61	2.80
	H3′*proS*–H3	7.21 (2.50)	0.00 (4.65)	1.93	2.86
	H3′*proS*–H5	12.84 (2.24)	0.00 (4.57)	5.10	5.10
	H3′*proR*–H2	0.00 (4.12)	3.36 (2.80)	1.28	2.02

[a] Noeprom value from a full-matrix cross peak intensity calculation extended to the AMBER* $^4C_1$ cluster. [b] Boltzmann-averaged distances between proton pairs. [c] Noeprom value from a full-matrix cross peak intensity calculation extended to the AMBER* $^1S_3$ cluster. [d] *J*-Fitted relative populations from Table 3. [e] Noeprom calculations for a cluster ratio corresponding to the fitted population in the preceding column. The agreement factor of NOE values relative to the experimental values are 0.89% for **1** and 0.54% for **2** (agreement factor is calculated as sum of deviations divided by sum of experimental values).

Table 5. Use of the experimental NOE intensities to estimate the relative population of the MM3* conformations.

Compound	Proton pair	Noeprom, MM3*, $^4C_1$, NOE (%)[a] (distance [Å])[b]	Noeprom, MM3*, $^1S_3$, NOE (%)[c] (distance [Å])[b]	Noeprom, MM3*, $^1C_4$, NOE (%)[d] (distance [Å])[b]	Exp. NOE (%)	MM3*, fitted NOE (%)[f]
NOE fitted ratio						$^4C_1$:$^1S_3$:$^1C_4$, 50:50:0 (*J*-fitted 48:25:27)[e]
1	H1–H4′	3.79 (2.60)	0.78 (3.22)	0.00 (4.07)	2.30	2.30
	H3′*proS*–H3	7.57 (2.47)	0.00 (3.89)	0.00 (5.40)	3.70	3.82
	H3′*proS*–H5	13.14 (2.22)	0.00 (4.28)	0.00 (4.51)	7.09	6.63
	H3–H5	4.21 (2.50)	2.25 (2.78)	0.00 (4.31)	3.24	3.24
	H1–H6*proR*	0.00 (4.91)	2.33 (2.70)	4.51 (2.39)	3.01	1.15
	H4′–H2	0.67 (3.44)	4.47 (2.57)	1.70 (3.00)	2.72	2.55
NOE fitted ratio						$^4C_1$:$^1S_3$:$^1C_4$, 21:79:0 (*J*-fitted 60:24:16)[e]
2	H1–H3′*proR*	2.57 (2.51)	4.31 (2.42)	3.96 (2.45)	3.94	3.94
	H1–H3′*proS*	3.51 (2.42)	1.53 (2.74)	1.86 (2.70)	0.43	1.95
	H1–H6*proR*	0.00 (4.87)	2.51 (2.67)	6.76 (2.28)	2.88	1.98
	H5–H3	3.71 (2.63)	2.76 (2.77)	0.00 (4.31)	3.43	2.96
	H4′–H3	7.88 (2.34)	2.28 (2.87)	0.00 (4.43)	2.14	3.46
	H6*proS*–H4	2.25 (2.87)	1.05 (3.20)	0.00 (4.02)	2.61	1.30
	H3′*proS*–H3	1.15 (3.19)	0.00 (4.43)	0.00 (5.37)	1.93	0.24
	H3′*proS*–H5	5.35 (2.51)	0.00 (4.52)	0.00 (4.53)	5.10	1.13
	H3′*proR*–H2	0.00 (4.08)	1.91 (3.04)	4.83 (2.64)	1.28	1.51

[a] Noeprom value from a full-matrix cross peak intensity calculation extended to the MM3* $^4C_1$ cluster. [b] Boltzmann-averaged distances between proton pairs. [c] Noeprom value from a full-matrix cross peak intensity calculation extended to the MM3* $^1S_3$ cluster. [d] Noeprom value from a full-matrix cross peak intensity calculation extended to the MM3* $^1C_4$ cluster. [e] *J*-Fitted relative populations from Table 3. [f] Noeprom calculations for a cluster ratio corresponding to the fitted population in the preceding column. The agreement factor of NOE values relative to the experimental values are 0.43% for **1** and 1.27% for **2**.

thus estimated are reported in Tables 4, 5 and 6 (NOE-fitted ratio columns) together with the NOE intensity values they originate from (NOE-fitted% NOE columns). *J*-fitted population estimates are also included in Tables 4–6, for comparison. The NOE data can be reproduced by all sets of fitted conformer populations with agreement factors ranging from 0.43% to 1.46% (see legends of Tables). Populations obtained by *J*-fitting or NOE-fitting do not differ significantly when the AMBER* (Table 4) or OPLSAA (Table 6) geometries are used. For instance, using AMBER*

Table 6. Use of the experimental NOE intensities to estimate the relative population of the OPLSAA conformations.

Compound	Proton pair	Noeprom, OPLSAA, $^4C_1$, NOE (%)[a], (distance [Å])[b]	Noeprom, OPLSAA, $^1C_4$, NOE (%)[c] (distance [Å])[b]	Exp., NOE (%)	OPLSAA, fitted NOE (%)[e]
NOE fitted ratio					$^4C_1$:$^1C_4$, 55:45 (*J*-fitted 60:40)[d]
1	H1–H4′	4.27 (2.56)	0.00 (3.70)	2.30	2.33
	H3′*proS*–H3	5.04 (2.66)	0.00 (4.96)	3.70	2.75
	H3′*proS*–H5	12.98 (2.25)	0.00 (4.06)	7.09	7.09
	H3–H5	3.20 (2.62)	0.00 (4.14)	3.24	1.75
	H1–H6*proR*	0.00 (4.54)	6.05 (2.32)	3.01	2.75
	H4′–H2	0.81 (3.31)	3.31 (2.69)	2.72	1.95
NOE fitted ratio					$^4C_1$:$^1C_4$, 76:24 (*J*-fitted 80:20) [d]
2	H1–H3′*proR*	2.15 (2.57)	4.27 (2.39)	3.94	2.65
	H1–H3′*proS*	3.59 (2.42)	1.62 (2.62)	0.43	3.13
	H1–H6*proR*	0.00 (5.02)	3.01 (2.54)	2.88	0.71
	H5–H3	3.76 (2.63)	0.00 (4.25)	3.43	2.88
	H4′–H3	6.20 (2.43)	0.00 (4.48)	2.14	4.74
	H6*proS*–H4	1.70 (2.96)	0.00 (3.86)	2.61	1.30
	H3′*proS*–H3	1.39 (3.12)	0.00 (5.35)	1.93	1.06
	H3′*proS*–H5	4.48 (2.55)	0.00 (4.47)	5.10	3.43
	H3′*proR*–H2	0.00 (4.05)	5.46 (2.61)	1.28	1.28

[a] Noeprom value from a full-matrix cross peak intensity calculation extended to the OPLSAA $^4C_1$ cluster. [b] Boltzmann-averaged distances between proton pairs. [c] Noeprom value from a full-matrix cross peak intensity calculation extended to the OPLSAA $^1C_4$ cluster. [d] *J*-Fitted relative populations from Table 3. [e] Noeprom calculations for a cluster ratio corresponding to the fitted population in the preceding column. The agreement factor of NOE values relative to the experimental values are 0.59% for **1** and 1.46% for **2**.

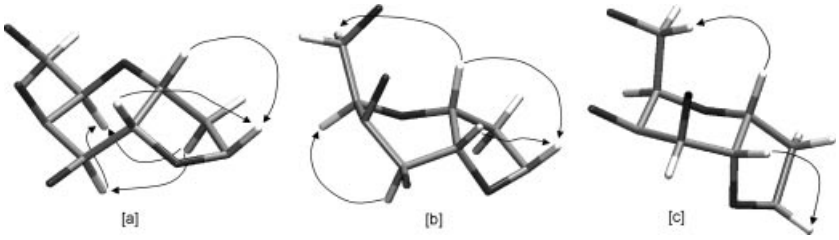

Figure 3. Illustration of NOE exclusive contacts for compound **1** (analogous considerations could be derived for compound **2**). Only MM3* cluster leaders are represented: [a] $^1C_4$, [b] $^1S_3$ and [c] $^4C_1$ cluster leaders.

geometries for both fitting procedures describes the system as an almost equimolar mixture of $^4C_1$ and $^1S_3$ conformations. On the contrary, when the MM3* geometries were used to fit the NOE intensity data, the best fit was obtained by excluding the $^1C_4$ inverted chair, that was still accepted by the *J*-fitting procedure (as 15% or 27% of the conformer population for **1** and **2**, respectively). Thus the analysis of the NOE contacts, which is more sensitive than the scalar coupling constant analysis to small changes in the three-dimensional structure of the systems examined, appears to suggest that a conformer distribution including $^4C_1$ and $^1S_3$ geometries only reproduces the experimental data better than a distribution which also includes the inverted $^1C_4$ chair.

For comparison, the agreement factors calculated directly using the MC/EM populations collected in Figure 2 are 2.83% (Amber*), 2.50% (MM3*) and 2.67% (OPLSAA) for compound **1** and the corresponding deviations for compound **2** are: 2.22%, 1.33% and 2.33% (for details, see Table SI-4 in the Supporting Information).

Conclusions

The structure and dynamics of **1** and **2** have proven hard to predict using computational methods. The experimental data could not be interpreted based upon a single conformation of the bicyclic structures. However, a combination of NMR spectroscopy and molecular modelling was finally able to define the three-dimensional structures and dynamics of these fluxional molecules in aqueous solution. We can also determine which of three well-known force fields are most reliable in reproducing the experimental observations and should therefore be used in design studies.

The NMR spectroscopic data suggested that the pyran ring in both molecules rapidly (on the NMR time scale)

interconverts between two ($^4C_1$, $^1S_3$) or three ($^4C_1$, $^1S_3$ and $^1C_4$) conformations and the data-fitting indicates that the canonical pyran $^4C_1$ chair represents about 50–60% of the total conformer population. Both NOE and *J* analysis concur in describing a fluxional system that samples at least two conformations for the pyran ring, a $^4C_1$ chair and a $^1S_3$ skew-boat, with a possible contribution fromthe $^1C_4$ inverted chair. However, a large presence of the latter conformer, which is predicted as the global minimum by the OPLSAA force field, is unlikely, on the basis of the medium-strong H3–H5 NOE cross peaks that could be observed for both **1** and **2**. Indeed, although the overall NOE fitting obtained using OPLSAA conformations is comparable with those obtained with MM3* or AMBER*, the intensity of the H3–H5 cross peak is very poorly reproduced using the two chairs only (Table 6, OPLSAA force field) and is much better reproduced using conformers of the $^4C_1$ and $^1S_3$ type (Table 4 and 5, AMBER* and MM3*). Indeed, NOE-fitted populations tend to exclude the $^1C_4$ inverted chair also when it is included in the initial population, as in the MM3* case (Table 5). Hence, OPLSAA, which yields an inverted chair as its global minimum, appears to be the least predictive of the force fields tested.

Both the other force fields examined, AMBER* and MM3*, can account for the experimentally observed NMR spectroscopic data, but MM3* is less accurate in the description of the C5–C6 extra-annular torsion. Neither AMBER* or MM3* potential energy surfaces directly yield an accurate representation of conformer distribution: AMBER* tends to over-represent the $^4C_1$ chair and MM3* the $^1S_3$ skew-boat. These errors are reflected in the poor reproduction of experimental results for both the 1,2-scalar couplings (*J*) and NOE intensities calculated directly from the modelling-derived populations using full-matrix approximations (Supporting Information Table SI-3 and SI-4). On the contrary, conformer distributions compatible with experimental results can be back-calculated by fitting the *J* and NOE experimental values with scalar couplings and (full-matrix approximated) NOE intensities calculated for single clusters of conformations originating from molecular modelling. It was shown that the populations calculated with the two fitting procedures are in full agreement starting from the AMBER* geometries, but NOE analysis tends to discount the $^1C_4$ inverted chair found by MM3* and retained by the *J*-fitting procedure.

The stereoisomeric bicyclic structures described in this paper largely retain the structural characteristics of natural galactosides, and yet, as C-glycosides, they are stabilized against chemical and enzymatic hydrolysis. Hence, they could be developed as drug-like ligands and inhibitors of galactose-binding proteins. Indeed, cholera toxin B5 pentamer, a paradigmatic example of a galactose receptor, binds to **1** and to galactose with similar affinity, as measured by fluorescence spectroscopy.[21] With the same approach, similar scaffolds could be obtained starting from different monosaccharides. The synthesis of these structures, which can be achieved in just four high-yielding steps, without the need for tedious protection-deprotection sequences, makes them very attractive for library design, or diversity-oriented synthetic projects.

Further studies are in progress to develop the synthetic potential of these structures.

Experimental Section

NMR Methods

NMR spectra were recorded in D_2O using Bruker AVANCE 400 and 500 spectrometers, at 293 K. 1D-, as well as 2D-, COSY, HSQC and NOESY experiments were recorded using the standard pulse sequences. NOESY experiments were carried out using mixing times of 600 ms and 800 ms. Exclusive NOE contacts for both compounds were identified and integrated from the NOESY spectra relative to the diagonal peak of the corresponding rows. Experimental scalar coupling constants, $^3J_{H–H}$, were extracted from signal splittings and compared with those estimated for the $^4C_1$, $^1C_4$ and skew-boat geometries calculated from the molecular mechanics calculations. Cross peaks from NOESY experiments were integrated using the MestReC software.[22] Their volumes were compared with those estimated for Bolztmann-averaging by Noeprom[19] using a full-matrix relaxation approach, as described below.

Computational Methods

All structures were investigated with MacroModel 8.1,[13] using GB/SA implicit water solvent,[12] constant dielectric and extended electrostatic treatment (8 Å for Van der Waals cut-off of interactions, and 20 Å as cut-off of electrostatic interactions). Calculations were performed using the AMBER*, OPLSAA and MM3* force fields.

A 10,000 step Monte Carlo/Multiple Minimization[16] was performed using 500 steps Polak–Ribiere Conjugate Gradient algorithm for minimization. All found minima converged to 0.05 kJ·A^{-1} for the gradient value. The pyran ring was allowed to open and a chirality check was added to avoid configuration changes. Other variables for the Monte Carlo search were the C–C, C–O and C–N single bonds. The orientations of the hydroxy groups were not included in the list of explicit variables. The results were analyzed taking into account all conformations found by each force field within the first 12.6 kJ/mol from the respective global minimum. The structures were clustered based on the conformation of the pyran ring ($^4C_1$ chair, $^1C_4$ inverted chair and $^1S_3$ skew-boat). Each cluster contains multiple conformations, which differ mainly by the puckering of the five-membered ring and by the orientation of the amide side-chain (see Supporting Information).

The NOE volumes were generated from the computational models using the Noeprom software[19] based on a full-matrix relaxation approach[18] and using a rigid isotropic model.[23] The NOE volumes reported in the Tables correspond to a 400 MHz spectrometer, using 0.8 s of mixing time and a correlation time of 60 ps. The fitting for the 500 MHz data and other mixing times produced basically the same conclusions as those reported here. The force field predictions were obtained as Boltzmann-weighted averages of all the conformations calculated by each force field within 12.6 kJ/mol from the global minimum. They are collated in Table SI-4 of the Supporting Information The cluster-averagedNnEe values in Table 4-Table 6 were calculated as Bolztmann distributions over the conformers belonging to individual clusters. These cluster-averaged NOE volumes were then used as input for the fitting processes.

Similarly, cluster averaged values of the scalar couplings $^3J_{H–H}$ were estimated using the empirical generalization of the Karplus equa-

tion proposed by Haasnoot et al.[20] as Boltzmann averages over the members of individual clusters. These cluster-averaged *J* values were used in the following fitting procedure to obtain *J*-fitted cluster populations.

Molecular dynamics calculations were performed with AMBER* and MM3* using stochastic dynamics (SD).[24] (Mixed-Mode Monte Carlo-stochastic dynamics[16] cannot be used for cyclic structures). Simulations were run for 1 ns, using the same force field, solvent and non-bonded interactions treatment used for the MC/MM search. The time step was set to 1 fs, the temperature to 300 K and the frictional coefficient to 0.5 ps^{-1}. Conformational sampling was done every pico-second. Under these conditions, SD simulations are not likely to have reached convergence; therefore, they were not used to extract the expected NOE intensities, but only used to assess the dynamic flexibility of the ring system (see Supporting Information).

Fitting Procedure

Fitting of the experimental $^3J_{H-H}$ values was obtained by using the Simplex algorithm.[25] An initial value was assigned to the weight of a given cluster and an estimation of the average scalar coupling calculated. Subsequently, the deviation between the calculated and experimental values was iteratively minimized (up to 10.000 steps) and thus, the best-fitting population weights were obtained. The same procedure was applied to estimate the fitted conformational distributions from NOE intensities.

Synthesis

General Procedures

All non-aqueous reactions were carried out in oven- or flame-dried glassware in an atmosphere of dry argon, unless otherwise noted. Except as otherwise indicated, all reactions were magnetically stirred and monitored by analytical thin-layer chromatography using Merck pre-coated silica gel plates with F254 indicator. Visualization was accomplished by UV light (256 nm), potassium permanganate, phosphomolybdic acid, 2,4-dinitrophenylhydrazone and/or *p*-anisaldehyde solution. Flash column chromatography was performed according to the method of Still using silica gel 60 (mesh 230–400) supplied by E. Merck. HPLC was performed on a Waters HPLC system (515 pumps); detector Waters 2487 dual wavelength using a Waters high performance carbohydrate 60 Å column. Yields refer to chromatographically and spectrographically pure compounds, unless otherwise noted. All solvents were reagent grade and dried from molecular sieves (4 Å) prior to use. All other reagents and starting materials, unless otherwise noted, were purchased from commercial vendors and used without further purification. All melting points were determined in Pyrex capillaries with a Thomas Hoover Unimelt melting point apparatus and are uncorrected. ^1H NMR and ^{13}C NMR spectra were recorded on a Varian 400 (400 MHz ^1H, 100 MHz ^{13}C) and on a Bruker Avance 500 (500 MHz ^1H, 100 MHz ^{13}C). Chemical shift values (δ) are reported in ppm relative to residual chloroform (δ = 7.27 ppm for ^1H; δ = 77.23 ppm for ^{13}C). The proton spectra are reported as follows: δ (multiplicity, number of protons, coupling constant *J*, assignment). Multiplicities are indicated by s (singlet), d (doublet), t (triplet), q (quartet), p (pentet), sx (sextet), h (heptet), o (octet), m (multiplet), br (broad) and appt (apparent). The identification of ^1H and ^{13}C signals was achieved using a combination of ^1H, ^{13}C, DEPT, COSY, NOESY experiments. Optical rotations were measured with a Perkin–Elmer model 241 polarimeter and reported as follows: $[\alpha]_D$ (c, solvent). $[\alpha]_D$ is reported in 10^{-1} deg cm^{-2} g^{-1}; concentration (c) is g in per 100 mL. High resolution electron spray ionization (ESI) mass spectra were obtained on a FT-ICR (APEXTM II Bruker Daltonics) at University of Milan.

1-(α-D-Galactopyranosyl)-2-propene (4): To a suspension of methyl-α-D-galactopyranoside (2.00 g, 0.01 mol) in acetonitrile (2.0 mL), bis(trimethylsilyl)trifluoroacetamide (BTSFA) (8.20 mL, 0.031 mol) was added and the resulting mixture heated at reflux for 1 h, when the mixture became clear and uniform. Allyltrimethylsilane (2.40 mL, 0.015 mol), followed by trimethylsilyl trifluoromethanesulfonate (0.92 mL, 5.00 mmol), was then added at 0 °C and the reaction mixture stirred for 18 h at room temp. After this time, the mixture was poured (CAUTION!) into ice-cold water and stirred for 3 h, prior to being neutralized (pH = 7) with IRN 78 resin, filtered through Celite and the filtrate concentrated under reduced pressure. The residue was purified by flash column chromatography over silica gel (EtOAc/MeOH, 15:1) affording **4** (1.78 g, 85%): white solid, m.p. 127–131 °C (EtOAc), $[\alpha]_D$ = +88.0 (1.0 g/dL, MeOH), R_f = 0.4 (EtOAc/MeOH, 4:1). ^1H NMR (400 MHz, CD_3OD, 25 °C): δ = 5.92–5.82 (m, 1 H, CH=CH_2), 5.14–5.01 (m, 2 H, CH=CH_2), 4.01–3.94 [m, 2 H, H(1), H(5)], 3.91–3.87 [dd, *J* = 5.2, 8.7 Hz, 1 H, H(2)] 3.77–3.71 [m, 3 H, H(4), H(6)], 3.69–3.66 [dd, *J* = 3.1, 8.7 Hz, 1 H, H(3)], 2.50–2.34 [m, 2 H, H(1′)] ppm. ^{13}C NMR (100 MHz, CD_3OD, 25 °C): δ = 139.4 (CH), 119.7 (CH_2), 78.6 (CH), 76.9 (CH), 74.7 (CH), 73.0 (CH), 72.9 (CH), 64.8 (CH_2), 33.9 (CH_2) ppm. MS-ESI: *m*/*z* 227.0889 $[[M + Na]^+$ calcd. for $C_9H_{14}O_5Na$ 227.0898].

(2*S*/*R*,3a*R*,5*R*,6*R*,7*S*,7a*R*)-5-Hydroxymethyl-2-iodomethyl-hexahydrofuro[3,2-*b*]pyran-6,7-diol (5): To a stirred solution of **4** (103 mg, 0.50 mmol) in DMF (8.0 mL), powder sodium hydrogen carbonate (168 mg, 2.00 mmol) and iodine (192 mg, 0.76 mmol) were sequentially added and the resulting mixture was stirred at room temp. for 12 h. Solid $Na_2S_2O_5$ (1.00 g) was then added to the red solution and after 1 h, the resulting pale-yellow solution filtered through a pad of Celite and the filtrate concentrated under reduced pressure. The residue was purified by flash column chromatography over silica gel (EtOAc/MeOH, 15:1) to provide **5** (139 mg, 85%) as a mixture of diastereomers: yellow oil, R_f = 0.6 (EtOAc/MeOH, 4:1). ^1H NMR (2.6:1 mixture of diastereomers, asterisks denote resonances from minor anomer, 400 MHz, CD_3OD, 25 °C): δ = 4.57–4.52 [m, H(3a), H(3a*)], 4.19–4.13 [m, H(2*)], 4.15–4.07 [m, H(2)], 3.97–3.95 [dd, *J* = 3.0, 4.0 Hz, H(6)], 3.96–3.95 [m, H(6*)], 3.94–3.91 [dd, *J* = 4.5, 5.3 Hz, H(7a)], 3.92–3.87 [m, H(7a*), H(7), H(7*)], 3.83–3.76 [m, H(5), H(5*), C*H*OH, C*H*OH*], 3.70–3.66 (dd, *J* = 3.8, 11.9 Hz, C*H*OH*), 3.69–3.65 (dd, *J* = 3.8, 11.6 Hz, C*H*OH), 3.36–3.33 (m, C*H*I, C*H*I*), 2.31–2.24 [m, H(3)], 2.23–2.18 [ddd, *J* = 2.6, 6.4 Hz, H(3*)], 1.97–1.90 [ddd, *J* = 4.2, 5.9 Hz, H(3)], 1.86–1.79 [m, H(3*)] ppm. ^{13}C NMR (100 MHz, D_2O, 25 °C): δ = 80.6* (CH), 79.1 (CH), 77.5 (CH), 76.8* (CH), 74.9* (CH), 74.5 (CH), 74.1 (CH), 73.3* (CH), 71.9 (CH), 69.7* (CH), 68.2 (CH), 68.0* (CH), 60.4 (CH_2), 59.9* (CH_2), 35.2* (CH_2), 34.6 (CH_2), 11.2* (CH_2), 10.3 (CH_2) ppm. MS-ESI: *m*/*z* 352.9856 $[[M + Na]^+$ calcd. for $C_9H_{15}IO_5Na$ 352.9846].

(2*S*/*R*,3a*R*,5*R*,6*R*,7*S*,7a*R*)-2-Azidomethyl-5-hydroxymethyl-hexahydrofuro[3,2-*b*]pyran-6,7-diol (6): To a stirred solution of bicyclic iodoethers **5** (360 mg, 1.09 mmol) in DMF (5.0 mL), a solution of freshly prepared tetrabutylammonium azide (nBu_4NN_3) (540 mg, 1.91 mmol) in DMF (3.0 mL) was added and the resulting mixture stirred at room temp. for 12 h and then concentrated under reduced pressure. The residue was then triturated in cold EtOAc, the resulting white precipitate filtered and the filtrate evaporated under reduced pressure. Purification of the obtained crude by flash column chromatography over silica gel (petroleum ether/EtOAc, 3:1) provided **6** (200 mg, 75%) as a mixture of diastereomers: yellow oil, R_f = 0.6 (EtOAc/MeOH, 4:1). ^1H NMR (2.4:1 mixture of anomers, asterisks denote resonances from minor anomer, 400 MHz, D_2O, 25 °C): δ = 4.54–4.48 [m, H(3a), H(3a*)], 4.32–4.48 [m, H(2*)],

4.14–4.06 [m, H(2)], 3.99–3.96 [dd, J = 5.2, 6.7 Hz, H(7a)], 3.84–3.52 [m, H(5), H(6), H(7), CH_2OH, H(5*), H(6*), H(7*), H(7a*), CH_2OH*], 3.46–3.40 (m, CHN$_3$, CHN$_3$*), 3.28–3.15 (m, CHN$_3$, CHN$_3$*), 2.12–2.02 [m, H(3), H(3*)], 1.88–1.78 [m, 2 H, H(3), H(3*)] ppm. ^{13}C NMR (100 MHz, CDCl3, 25 °C): δ = 82.0* (CH), 81.8 (CH), 76.9 (CH), 76.8* (CH), 74.64* (CH), 74.6 (CH), 73.4 (CH), 71.5 (CH), 70.4* (CH), 68.5 (CH), 61.4 (CH$_2$), 54.8 (CH$_2$), 34.1 (CH$_2$) ppm. MS-ESI: m/z 268.0904 [[M + Na]$^+$ calcd. for $C_9H_{15}N_3O_5Na$ 268.0916].

(2*R*,3a*R*,5*R*,6*R*,7*S*,7a*R*)-*N*-(6,7-Dihydroxy-5-hydroxymethyl-hexahydrofuro[3,2-*b*]pyran-2-ylmethyl)acetamide (1) and (2*S*,3a*R*,5*R*,6*R*,7*S*,7a*R*)-*N*-(6,7-Dihydroxy-5-hydroxymethyl-hexahydrofuro[3,2-*b*]pyran-2-ylmethyl)acetamide (2): To a solution of bicyclic azides **6** (80 mg, 0.32 mmol) and acetic anhydride (80 mL, 0.84 mmol) in MeOH (2 mL), Pd(OH)$_2$/C (20%, 160 mg, 10% by weight) was added at room temp. The reaction mixture was then placed under an atmosphere of H_2 and stirred for 24 h. The mixture was then filtered through Celite and the filtrate evaporated under reduced pressure. The residue was purified by flash column chromatography over silica gel (EtOAc/MeOH, 4:1) to provide **1** and **2** (60 mg, 70%): colorless oil, R_f = 0.2 (EtOAc/MeOH, 4:1) as a mixture of diastereomers. This oil was further submitted to separation via preparative HPLC (H_2O/CH_3CN, 1:1) to provide pure **1** (37 mg) and **2** (15 mg).

1: $[\alpha]_D$ = +24.36 (0.9 g/dL, MeOH). ^{1}H NMR (500 MHz, D_2O, 25 °C, numbering as in Figure 1): δ = 4.59 [q, J = 6.6 Hz, 1 H, H(1)], 4.10 [m, J = 7.8, 6.8, 4.3 Hz, 1 H, H(4′)], 3.95 [t, J = 2.8 Hz, 1 H, H(4)], 3.89 [t, J = 6.4 Hz, 1 H, H(2)], 3.87 [m, J = 8.9, 3.7 Hz, 1 H, H(5)], 3.78 [q, J = 11.9, 8.5 Hz, 1 H, H(6)], 3.73 [q, J = 6.8, 2.8 Hz, 1 H, H(3)], 3.65 [q, J = 11.8, 3.5 Hz, 1 H, H(6)], 3.35 [m, J = 14.2, 6.4, 4.4 Hz, 2 H, H(5′)], 2.20 [sx, J = 13.3, 6.8 Hz, 1 H, H(3′)], 1.97 (s, 3 H, CH_3), 1.80 [sx, J = 13.3, 7.8 Hz, 1 H, H(3′)] ppm. ^{13}C NMR (100 MHz, D_2O, 25 °C): δ = 79.2 (CH), 76.8 (CH), 74.8 (CH), 73.7 (CH), 71.9 (CH), 68.1 (CH), 60.5 (CH$_2$), 44.5 (CH$_2$), 32.1 (CH$_2$), 22.3 (CH$_3$) ppm. HRMS (ESI): calcd. for $C_{11}H_{19}NO$ [M + Na]$^+$: 284.11101, found [M + Na]$^+$: 284.10908.

2: $[\alpha]_D$ = +13.89 (0.3 g/dL, MeOH). ^{1}H NMR (500 MHz, D_2O, numbering as in Figure 1): δ = 4.56 [m, 1 H, H(1)], 4.28 [m, 1 H, H(4′)], 4.02 [q, J = 6.7, 5.9 Hz, 1 H, H(2)], 3.94 [t, J = 3.0 Hz, 1 H, H(4)], 3.85 [sx, J = 8.5, 3.5 Hz, 1 H, H(5)], 3.77 [q, J = 11.8, 8.5 Hz, 1 H, H(6)], 3.76 [q, J = 6.6, 3.0 Hz, 1 H, H(3)], 3.62 [q, J = 11.8, 3.5 Hz, 1 H, H(6)], 3.27 [m, 2 H, H(5′)], 2.09 [o, J = 12, 7.3, 5 Hz, 1 H, H(3′)], 1.97 (s, 3 H, CH3), 1.79 [sx, J = 14, 7 Hz, 1 H, H(3′)] ppm. ^{13}C NMR (100 MHz, D_2O, 25 °C): δ = 79.7 (CH), 75.9 (CH), 74.8 (CH), 73.0 (CH), 69.5 (CH), 67.9 (CH), 59.6 (CH$_2$), 42.7 (CH$_2$), 31.9 (CH$_2$), 31.8 (CH$_3$) ppm. HRMS (ESI): calcd. for $C_{11}H_{19}NO_6$ [M + Na]$^+$: 284.11101, found [M + Na]$^+$: 284.10863.

Supporting Information (see also the footnote on the first page of this article): Details on conformational analysis of compounds **1** and **2** are collected in Tables SI-1-SI-4 and Figures SI-1-SI-7. Clustering and fitting procedures, including analysis of side-chain orientations, are collected in Tables SI-5 and SI-6.

Acknowledgments

The project was supported by the European Programme Improving Human Potential under contract HPRN–CT–2002–00173 (Glycidic Scaffolds Network).

[1] L. Cipolla, F. Peri, B. La Ferla, C. Redaelli, F. Nicotra, *Curr. Org. Synth.* **2005**, *2*, 153.
[2] S. A. Gruner, E. Locardi, E. Lohof, H. Kessler, *Chem. Rev.* **2002**, *102*, 491–514.
[3] G. T. Le, G. Abbenante, B. Becker, M. Grathwohl, J. Halliday, G. Tometzki, J. Zuegg, W. Meutermans, *Drug Discovery Today* **2003**, *8*, 701–709.
[4] S. F. Oliver, C. Abell, *Curr. Opin. Chem. Biol.* **1999**, *3*, 299–306.
[5] J. A. Bennek, G. R. Gray, *J. Org. Chem.* **1987**, *52*, 892–897.
[6] H. J. G. Broxterman, P. A. Kooreman, H. van den Elst, H. C. P. F. Roelen, G. A. van der Marel, J. H. van Boom, *Recl. Trav. Chim. Pays-Bas* **1990**, *109*, 583–590.
[7] In the original paper 5 equiv. of TMSOTf and 5 equiv. of TMAll were used.
[8] L. Lay, L. Cipolla, B. La Ferla, F. Peri, F. Nicotra, *Eur. J. Org. Chem.* **1999**, 3437–3440.
[9] L. Cipolla, L. Lay, F. Nicotra, *J. Org. Chem.* **1998**, *62*, 6678–6681.
[10] J. L. Asensio, J. Jimenez-Barbero, *Biopolymers* **1995**, *35*, 55–73.
[11] S. Pérez, A. Imberty, S. B. Engelsen, J. Gruza, K. Mazeau, J. Jimenez-Barbero, A. Poveda, J. F. Espinosa, B. P. van Eyck, G. Jonhson, A. D. French, M. L. C. E. Kouwijzer, D. J. Grootenhuis, A. Bernardi, L. Raimondi, H. Senderowitz, V. Durier, G. Vergoten, K. Rasmussen, *Carbohydr. Res.* **1998**, *314*, 141–155.
[12] W. C. Still, A. Tempczyk, R. C. Hawley, T. Hendrickson, *J. Am. Chem. Soc.* **1990**, *112*, 6127–6129.
[13] F. Mohamadi, N. G. J. Richards, W. C. Guida, R. Liskamp, M. Lipton, C. Caufield, G. Chang, T. Hendrickson, W. C. Still, *J. Comput. Chem.* **1990**, *11*, 440–467.
[14] M. K. Dowd, A. D. French, P. J. Reilly, *Carbohydr. Res.* **1994**, *264*, 1–19.
[15] H. Senderowitz, C. Parish, W. C. Still, *J. Am. Chem. Soc.* **1996**, *118*, 2078–2086.
[16] H. C. Kolb, B. Ernst, *Chem. Eur. J.* **1997**, *3*, 1571–1578.
[17] A. Bérces, D. M. Whitfield, T. Nukada, *Tetrahedron* **2001**, *57*, 477–491.
[18] B. A. Borgias, T. L. James, *Methods Enzymol.* **1989**, *176*, 169–183.
[19] Noeprom software is downloadable for free at http://desoft03.usc.es/mmartin/rmnweb/rmnexp_software.html.
[20] C. A. G. Haasnoot, F. A. A. M. de Leeuw, C. Altona, *Tetrahedron* **1980**, *36*, 2783–2792.
[21] Ingrid Velter, unpublished results.
[22] www.mestrec.com.
[23] G. Lipari, A. Szabo, *J. Am. Chem. Soc.* **1982**, *104*, 4546–4559.
[24] F. Guarnieri, W. C. Still, *J. Comput. Chem.* **1994**, *15*, 1302–1310.
[25] G. B. Dantzig, *Linear Programming and Extensions*; Princeton University Press: Princeton, New Jersey, **1963**.

Received: December 29, 2005
Published Online: May 8, 2006

